DOI: 10.1002/asia.201301331

Cobalt Complexes with Pyrazole Ligands as Catalyst Precursors for the Peroxidative Oxidation of Cyclohexane: X-ray Absorption Spectroscopy Studies and Biological Applications

Telma F. S. Silva,[a] Luísa M. D. R. S. Martins,[a, b] M. Fátima C. Guedes da Silva,[a, c] Maxim L. Kuznetsov,[a] Alexandra R. Fernandes,[a, c, d] Ana Silva,[c] Chun-Jern Pan,[e] Jyh-Fu Lee,[f] Bing-Joe Hwang,[e, f] and Armando J. L. Pombeiro*[a]

Abstract: $[CoCl(\mu\text{-}Cl)(Hpz^{Ph})_3]_2$ (**1**) and $[CoCl_2(Hpz^{Ph})_4]$ (**2**) were obtained by reaction of $CoCl_2$ with $HC(pz^{Ph})_3$ and Hpz^{Ph}, respectively (Hpz^{Ph} = 3-phenylpyrazole). The compounds were isolated as air-stable solids and fully characterized by IR and far-IR spectroscopy, MS(ESI+/−), elemental analysis, cyclic voltammetry (CV), controlled potential electrolysis, and single-crystal X-ray diffraction. Electrochemical studies showed that **1** and **2** undergo single-electron irreversible $Co^{II} \rightarrow Co^{III}$ oxidations and $Co^{II} \rightarrow Co^{I}$ reductions at potentials measured by CV, which also allowed, in the case of dinuclear complex **1**, the detection of electronic communication between the Co centers through the chloride bridging ligands. The electrochemical behavior of models of **1** and **2** were also investigated by density functional theory (DFT) methods, which indicated that the vertical oxidation of **1** and **2** (that before structural relaxation) affects mostly the chloride and pyrazolyl ligands, whereas adiabatic oxidation (that after the geometry relaxation) and reduction are mostly metal centered. Compounds **1** and **2** and, for comparative purposes, other related scorpionate and pyrazole cobalt complexes, exhibit catalytic activity for the peroxidative oxidation of cyclohexane to cyclohexanol and cyclohexanone under mild conditions (room temperature, aqueous H_2O_2). In situ X-ray absorption spectroscopy studies indicated that the species derived from complexes **1** and **2** during the oxidation of cyclohexane (i.e., Ox-**1** and Ox-**2**, respectively) are analogous and contain a Co^{III} site.

Complex **2** showed low in vitro cytotoxicity toward the HCT116 colorectal carcinoma and MCF7 breast adenocarcinoma cell lines.

Keywords: cobalt · cyclic voltammetry · cyclohexane oxidation · in vitro cytotoxicity · pyrazole based ligands · X-ray absorption spectroscopy

Introduction

Scorpionates are well-established ligands, and their complexes have made important contributions in bioinorganic modeling and catalysis.[1,2] The popularity of scorpionate systems stems, in large part, from their flexibility that allows the electronic and steric features at a metal center to be tuned, for example, by substitution at the apical atom or the atom at the 3-, 4-, or 5-position of the pyrazolyl rings. In particular, tris(pyrazol-1-yl)methane-type scorpionates XC-

[a] Dr. T. F. S. Silva, Prof. L. M. D. R. S. Martins, Prof. M. F. C. Guedes da Silva, Dr. M. L. Kuznetsov, Prof. A. R. Fernandes, Prof. A. J. L. Pombeiro
Centro de Química Estrutural, Instituto Superior Técnico
Universidade de Lisboa
Av. Rovisco Pais, 1049-001 Lisboa (Portugal)
Fax: (+351) 218464455
E-mail: pombeiro@tecnico.ulisboa.pt

[b] Prof. L. M. D. R. S. Martins
Chemical Engineering Department, ISEL
R. Conselheiro Emídio Navarro, 1959-007 Lisboa (Portugal)

[c] Prof. M. F. C. Guedes da Silva, Prof. A. R. Fernandes, A. Silva
Universidade Lusófona de Humanidades e Tecnologias
ULHT Lisbon
Campo Grande 376, 1749-024 Lisboa (Portugal)

[d] Prof. A. R. Fernandes
Departamento de Ciências da Vida
Faculdade de Ciências e Tecnologias
Universidade Nova de Lisboa
2829-516 Caparica (Portugal)

[e] Dr. C.-J. Pan, Prof. B.-J. Hwang
Nano Electrochemistry Laboratory
Department of Chemical Engineering
National Taiwan University of Science and Technology
Taipei 106 (Taiwan)

[f] Dr. J.-F. Lee, Prof. B.-J. Hwang
Nano Electrochemistry Laboratory
Department of Chemical Engineering
National Taiwan University of Science and Technology
Taipei 106 (Taiwan)

Supporting information for this article is available on the WWW under http://dx.doi.org/10.1002/asia.201301331.

$(Rpz)_3$ (pz = pyrazol-1-yl, R = H or substituent at the pz ring, X = H or substituent), which are much less studied than the related tris(pyrazol-1-yl)borates,[2] constitute an emerging field of research[2b–d] and provide a suitable entry for a fruitful coordination chemistry.

In pursuit of our ongoing work on the coordination chemistry of $HC(Rpz)_3$ and derivatives[3] and on the application of their complexes as catalysts for the partial oxidation of alkanes[3c,f–h,j,k,p–t] and as cytotoxic agents (including some Co complexes),[4] we have now selected sterically hindered phenyl-substituted tris(pyrazol-1-yl)methane, $HC(pz^{Ph})_3$; studied its coordination behavior at a cobalt(II) center; investigated the catalytic ability of the derived complexes (and related ones) for the peroxidative (by aqueous H_2O_2) oxidation of cyclohexane to cyclohexanol and cyclohexanone at room temperature; investigated the catalytic reaction mechanism by X-ray absorption spectroscopy (XAS) studies; and tested the in vitro cytotoxic activity for the water-soluble compounds in two human cancer cell lines, HCT116 colorectal and MCF-7 breast cancer carcinomas, and in one normal human fibroblast cell line.

Knowing that extended X-ray absorption fine structure (EXAFS) studies can provide relevant structural information that can be valuable to the identification of the intermediates in complex reaction,[5] we also applied in this study such a technique to our systems. To our knowledge, the application of EXAFS to the mechanistic study of alkane oxidation had not yet been reported.

Moreover, cobalt complexes can be fairly soluble in water if bearing a suitable substituent. The cytotoxic studies were justified by interest in cobalt complexes in experimental cancer therapy research on account of their role as systemic anticancer agents and their ability to undergo redox-dependent targeting of the malignant tissue of solid tumors.[4,6–11] Moreover, we recently found[4] that some Co–scorpionate complexes present moderate cytotoxicity toward HCT116 colorectal and HepG2 hepatocellular carcinoma human cancer cell lines.

Results and Discussion

Synthesis of Complexes and Spectroscopic Characterization

Reaction of $HC(pz^{Ph})_3$ (in stoichiometric amount) with $CoCl_2$ led to the dinuclear 3-phenylpyrazole complex with chloride bridges $[CoCl(\mu\text{-}Cl)(Hpz^{Ph})_3]_2$ (Hpz^{Ph} = 3-phenylpyrazole) (**1**; reaction a, Scheme 1). The formation of **1** involves $C(sp^3)$–N(pyrazolyl) bond rupture in $HC(pz^{Ph})_3$. Other cases of metal-induced cleavage of such types of bonds have been reported, namely, in $HC(pz)_3$ and $HC(3,5\text{-}Me_2pz)_3$ by the benzoylhydrazido rhenium(V) chelate $[ReCl_2\{\eta^2\text{-}N,O\text{-}N_2C(O)Ph\}(PPh_3)_2]$[3n] or triethylvanadate,[3f] and in bis(pyrazolyl)propane $(CH_3)_2C(pz)_2$ by Pt^{II} complexes[12] such as $[PtCl_2(RCN)_2]$ (R = Me or Ph) or $K_2[PtCl_4]$. Such behavior, to our knowledge, has not been previously shown for cobalt. In all the reported cases, the way the bond cleavage reaction occurs has not been established.

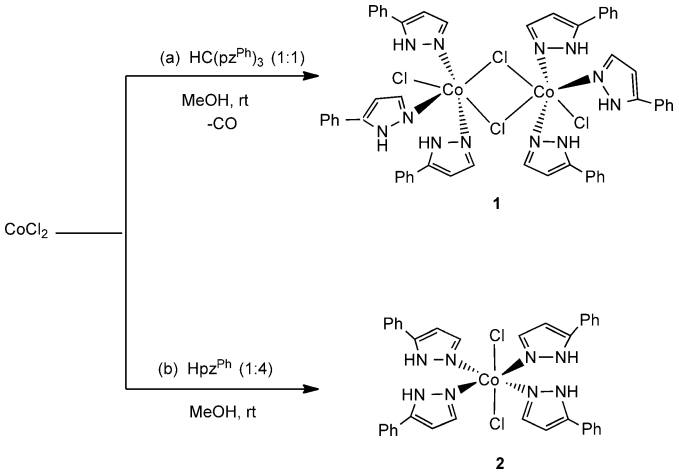

Scheme 1. Formation of Co^{II} complexes with 3-phenylpyrazole ligands.

Nevertheless, in our case it can be envisaged to involve overall metal-promoted hydrolysis of $HC(pz^{Ph})_3$ to yield three (per metal) ligated Hpz^{Ph} and CO. Interestingly, **1** could not be obtained upon reaction of $CoCl_2$ with Hpz^{Ph} (1:4) under the same conditions. The mononuclear complex $[CoCl_2(Hpz^{Ph})_4]$ (**2**) was formed instead (reaction b, Scheme 1) from the reaction mixture of those reagents in methanol at room temperature.

The complexes were characterized by elemental analysis, IR spectroscopy, ESIMS, cyclic voltammetry (CV), controlled potential electrolysis, and single-crystal X-ray diffraction analysis. Their IR spectra display ν(C=C) and ν(C=N) bands for the pyrazole groups in the normal range[3f,n,o] of 1626–1510 cm^{-1}. For **1**, the medium-intensity ν(Co–Cl) bands in the 312–275 cm^{-1} range confirm the presence of chloride ligands.

X-ray Molecular Structures

The ellipsoid plots of complexes **1** and **2** are depicted in Figures 1 and 2 with selected bonding parameters in the respective legends. Crystallographic data are given in Table 1. The geometries around the cobalt ions are of octahedral type. The asymmetric unit of **1** comprises half of the complex molecule, and the dinuclear species (Figure 1) contains an inversion center in the center of the planar $Co_2(\mu\text{-}Cl)_2$ core. The molecular geometry is that of a typical edge-sharing bioctahedron with a Co···Co^i intramolecular distance of 3.659(2) Å. The equatorial positions in each octahedron are occupied by the N5 atom from a phenylpyrazole ligand, the terminal chloride anion, and the bridging chlorides; the two octahedra share the common $Cl1–Cl1^i$ edge. The apical positions are taken up by the N1 and N3 atoms from two phenylpyrazole groups. A sticking feature in the structure of **2** concerns the elongated Co–Cl distances [2.6168(10) and 2.6996(10) Å] relative to those in **1**, for which this parameter ranges from 2.49 to 2.52 Å; this provides evidence for axial Jahn–Teller distortion and agrees with a low-spin Co^{II} configuration supported by DFT calculations. Whereas the phe-

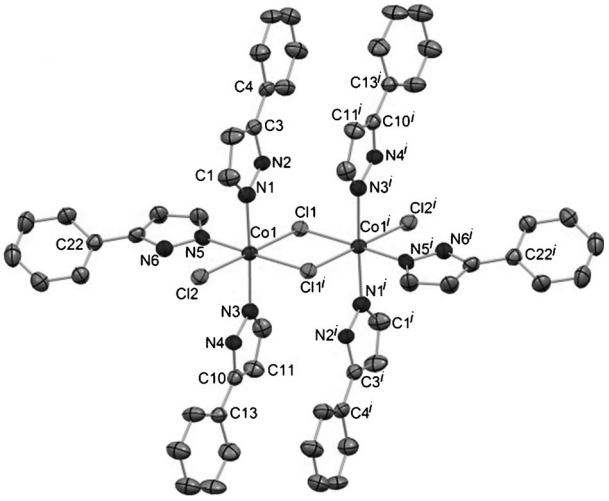

Figure 1. Crystal structure of complex **1** with atomic numbering scheme (ellipsoid probability level of 30%). Hydrogen atoms are omitted for clarity. Selected bond lengths [Å] and angles [°]: Cl1–Co1 2.523(2), Cl2–Co1 2.493(2), Co1–Cl1^i 2.505(2), N1–Co1 2.098(7), N3–Co1 2.095(6), N5–Co1 2.144(6), N1–N2 1.360(8), N3–N4 1.352(7), N5–N6 1.354(8); N1–Co1–N5 88.8(2), N3–Co1–N1 177.7(3), N3–Co1–N5 89.3(2), N3–Co1–Cl1^i 90.01(17), Cl2–Co1–Cl1 179.44(8), Cl1–Co1–Cl1^i 86.61(6). Symmetry operations to generate equivalent atoms: i: $-x$, $2-y$, $1-z$.

Table 1. Crystallographic data for compounds $[CoCl(\mu\text{-}Cl)(Hpz^{Ph})_3]_2$ (**1**) and $[CoCl_2(Hpz^{Ph})_4]$ (**2**).

	1	**2**
empirical formula	$C_{54}H_{48}C1_4Co_2N_{12}$	$C_{36}H_{32}Cl_2CoN_8$
formula weight	1124.70	706.53
crystal system	monoclinic	triclinic
space group	$P2_1/c$	$P\bar{1}$
a [Å]	11.7708(16)	9.3906(7)
b [Å]	18.023(2)	12.6240(9)
c [Å]	15.4269(16)	15.4387(11)
α [°]	90	110.582(5)
β [°]	126.075(7)	100.882(4)
λ [°]	90	99.238(2)
V [Å^3]	2645.2(6)	1630.5(2)
Z	2	2
T [K]	293(2)	150(2)
density (calcd) [Mg m^{-3}]	1.412	1.439
μ [mm^{-1}]	0.878	0.731
F(000)	1156	730
reflns. collected/unique/observed	34160/4837/2619	14889/5768/3970
R_{int}	0.116	0.0416
$R1$[a] ($I \geq 2\sigma$)	0.0788	0.0445
$wR2$[b] ($I \geq 2\sigma$)	0.1650	0.1189
goodness-of-fit on F^2	1.108	0.915

[a] $R1 = \Sigma||F_o|-|F_c||/\Sigma|F_o|$. [b] $wR2 = [\Sigma[w(F_o^2-F_c^2)^2]/\Sigma[w(F_o^2)^2]]^{1/2}$

nylpyrazole moieties that are perpendicular to the metallacycle are almost planar (the phenyl rings make angles of ≈6° with the plane of the attached pyrazoles), the others are substantially twisted, and the planes of the phenyl rings and the attached pyrazoles form an angle of 26°. This structure is stabilized by weak intramolecular hydrogen bonds [shortest d(D···A) = 3.051(6) Å; ∢(DHA) = 126.00°] involving the pyrazole N2-H2A, N4-H4, and N6-H6A as donor atoms and the chloride anions (either bridging or terminal) as acceptors, which results in an infinite chain running along the crystallographic a axis with the shortest Co···Co^i intramolecular distance of 8.509(2) Å. There are also intramolecular π···π stacking contacts: the N1–N2 and N3–N4 pyrazole rings are mutually involved in an almost face-to-face interaction with a distance of 3.903 Å between the ring centroids; the same occurs with the correspondingly attached phenyl rings, the centroids of which are 4.229 Å apart. Moreover, the H11 hydrogen atom (of the N3–N4 pyrazole ring) is directed toward the C22>C27 phenyl π cloud of a vicinal dimer (H11···centroid 2.990 Å, C11–H11···centroid 165.00°).

Interestingly, none of the phenylpyrazoles in the structure of **2** (Figure 2) presents coplanarity between the pyrazole and the attached phenyl ring, and the utmost bite angle of 53.42° was found in the N4–pyrazole-containing moiety. An-

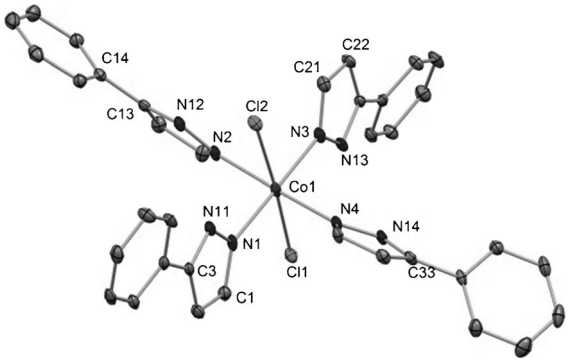

Figure 2. Crystal structure of complex **2** with atomic numbering scheme (ellipsoid probability level of 30%). Hydrogen atoms are omitted for clarity. Selected bond lengths [Å] and angles [°]: N1–Co1 2.081(3), N2–Co1 2.104(3), N3–Co1 2.072(3), N4–Co1 2.091(3), N1–N11 1.396(4), N2–N12 1.393(4), N3–N13 1.388(4), N4–N14 1.342(4), Cl1–Co1 2.6168(10), Cl2–Co1 2.6996(10); N3–Co1–N1 177.99(11), N4–Co1–N2 177.95(11), Cl1–Co1–Cl2 176.96(3).

other striking feature is the pairing of the molecules (Figure S1, Supporting Information) by means of medium/strong hydrogen bonds between the pyrazole N14 of one molecule as an H-donor and Cl1 from a vicinal molecule as the acceptor. Extensive π···π and H···π interactions are also present in the structure of **2**, which lead to a shorter Co···Co^i intermolecular distance [7.0049(8) Å] than that in **1**.

Electrochemical Studies

In view of the potential application of **1** and **2** as catalysts in oxidation processes and/or antitumor agents (see below), their redox properties were studied by CV and controlled potential electrolysis (CPE). For comparative purposes, the redox potentials of other related Co–scorpionate complexes are also included: $[Co(OSO_3H)(OCH_3)(HOCH_3)\{HC(pz)_3\}]$ (**3**), $[Co\{HOCH_2C(pz)_3\}_2](NO_3)_2$ (**4**), $[Co\{HOCH_2C(pz)_3\}_2][Co\{HOCH_2C(pz)_3\}(H_2O)_3]_2(Cl)_6{\cdot}6H_2O$ (**5**), $[CoCl_2(H_2O)\{PyCH_2OCH_2C(pz)_3\}]$ (**6**), and $[CoCl_2(H_2O)\{CH_3SO_2OCH_2C(pz)_3\}]$ (**7**).

By CV at a Pt disc electrode, in 0.2 M [nBu$_4$N][BF$_4$]/NCMe solution, mononuclear **2** exhibited a single-electron irreversible reduction wave at $^{I}E^{red}_{p/2}$ −0.64 V versus the saturated calomel electrode (SCE)standar assigned to the $Co^{II}\rightarrow Co^{I}$ reduction process and a single-electron irreversible oxidation wave, which concerns $Co^{II}\rightarrow Co^{III}$ oxidation, at $^{I}E^{ox}_{p/2}$ 1.36 V versus SCE (Table 2). Moreover, **1**, with two Co centers, displays two irreversible single-electron oxidation and reduction waves (Figure 3), which could be evidence of electronic communication between the cobalt centers through the bridging chloride ligands. The redox potentials of **1** and **2** are comparable to those shown by the related chlorido–Co complexes **6** and **7** (Table 2).

Table 2. Cyclic voltammetry data[a] for the cobalt complexes.

Compound	$^{I}E^{red}_{p/2}$	$^{II}E^{red}_{p/2}$	$^{I}E^{ox}_{p/2}\left(^{I}E^{ox}_{1/2}\right)$	$^{II}E^{ox}_{p/2}$	Ref.
1	−0.75	−1.22	1.36	1.88	this work
2	−0.64	–	1.52	–	this work
3[b,c]	−0.40		1.03	–	[4]
4[b]	−0.68		(0.58)	–	[4]
5[b]	−0.67	−1.21	(0.60)	1.20	[4]
6[b]	−0.60		1.28	–	[4]
7[b]	−0.64		1.10	–	[4]

[a] Values in V ± 0.02 relative to SCE; scan rate of 200 mV s^{-1} in 0.2 M [nBu$_4$N][BF$_4$]/NCMe unless stated otherwise. [b] For comparative purposes: [Co(OSO$_3$H)(OCH$_3$)(HOCH$_3$){HC(pz)$_3$}] (**3**), [Co{HOCH$_2$C(pz)$_3$}$_2$](NO$_3$)$_2$ (**4**), [Co{HOCH$_2$C(pz)$_3$}$_2$][Co{HOCH$_2$C(pz)$_3$}(H$_2$O)$_3$]$_2$(Cl)$_6$·6H$_2$O (**5**), [CoCl$_2$(H$_2$O){PyCH$_2$OCH$_2$C(pz)$_3$}] (**6**), and [CoCl$_2$(H$_2$O){CH$_3$SO$_2$OCH$_2$C(pz)$_3$}] (**7**). [c] In 0.2 M [nBu$_4$N][BF$_4$]/DMSO.

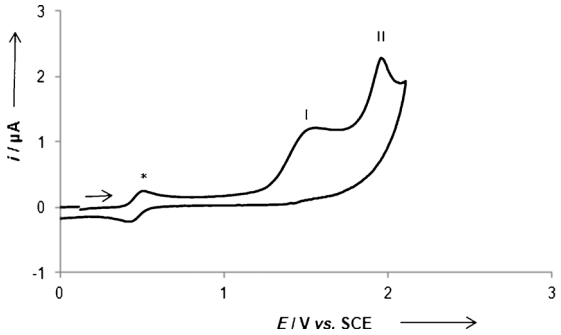

Figure 3. Cyclic voltammogram (anodic part) of **1** at a Pt disc electrode in a 0.20 M [nBu$_4$N][BF$_4$]/NCMe solution. Complex concentration: 1.5 mM. * = [Fe(η^5-C$_5$H$_5$)$_2$]$^{0/+}$ (internal standard).

As established by theoretical calculations (see below), although the oxidation process is initially mainly located at the ligands, upon geometry relaxation it becomes mostly metal centered to form a mixed-valence Co^{II}/Co^{III} species. Yet, the reductions are mainly positioned in the metal centers, and the presence of a mixed-valence Co^{II}/Co^{I} compound is not disregarded. However, the irreversibility of the waves (both oxidation and reduction waves), which indicate the involvement of chemical reactions following the electrode processes, did not allow estimation of the comproportionation constant for any of the mixed-valence complexes. The loss of the Cl^- ligands upon reduction, as suggested below by theoretical calculations, can account for the irreversibility.

The occurrence of single-electron oxidations (or reductions) was confirmed by exhaustive controlled potential electrolysis at a potential slightly anodic (or cathodic) to the corresponding peak potential. No redox process for free HC(pz^{Ph})$_3$ or Hpz^{Ph} was detected under the experimental conditions of this study.

The values of the $Co^{II/III}$ oxidation potential of the complexes are expected[13] to reflect the electron-donor characters of their ligands. The higher oxidation potential of **2** (bearing four bound 3-phenyl-substituted pyrazoles, Hpz^{Ph}, and two chloride ligands) than that of **1** (with three Hpz^{Ph} and three chloride ligands) reflects the expected weaker electron-donor character of Hpz^{Ph} than that of Cl^-. In fact, the latter ligand presents a lower value of the electrochemical lever E_L ligand parameter [$E_L = -0.24$ V vs. standard hydrogen electrode (NHE)][13a] than that of Hpz^{Ph} (which, although not yet reported, should be greater than that of the unsubstituted pyrazole, i.e., 0.20 V vs. NHE[13a]). One should note that E_L is a measure of the electron-donor character of a ligand: the stronger this character, the lower the value of E_L.

Compound **7**, which bears the methylsulfonate C-functionalized scorpionate ligand, presents a lower oxidation potential ($^{I}E^{ox}_{1/2} = 1.10$ V)[4] than **6** ($E^{ox}_{1/2} = 1.28$ V vs. SCE),[4] which indicates that the electron-acceptor character of the PyCH$_2$ group is stronger than that of CH$_3$SO$_2$.

The oxidation potentials of **1** and **2** are higher than those of other boron–scorpionate Co^{II} complexes with two phenyl groups at each pyrazolyl ring, for example, [Co(Tp^{Ph2})(acac)] (Tp^{Ph2} = tris-3,5-diphenylpyrazolylborate, acac = acetylacetonate), [Co(Tp^{Ph2})(dbm)] (dbm = 1,3-diphenylpropane-1,3-dionate), and [Co(Tp^{Ph2})(tmhd)] (tmhd = 2,2,6,6-tetramethylhepatane-3,5-dionate), with $E^{ox}_p = 1.19$, 1.27, and 1.36 V, respectively.[14]

The discussion of possible relations between, on the one side, the oxidation potential and, on the other side, the catalytic activity and the bioactivity are discussed below.

Theoretical DFT Calculations

Neutral Complexes

With aim to interpret the electrochemical behavior of the species under study, theoretical DFT calculations of model complexes **1′** and **2′** with unsubstituted pyrazolyl ligands instead of the phenyl-substituted ones were performed. The ground state of **2′** is quartet, which is 6.8 kcal mol^{-1} lower in energy than the doublet state. The high-spin septet ($S = 3$) configuration of **1′** was found to be the ground state, whereas the energy of the fully optimized low-spin broken symmetry (BS) state was slightly higher. The magnetic coupling parameter J calculated by using Equations (2) and (3) is +13.9 cm^{-1}, which is indicative of rather weak ferromagnetic coupling between two Co^{II} centers in this complex.

The calculated equilibrium structures of **1′** and **2′** in their ground states resemble the experimental structures of **1** and **2**, respectively. The maximum deviation between the main calculated and experimental bond lengths is 0.02–0.06 Å for the Co–Cl bonds in both **1** and **2** and for the Co–N bonds in **1**, whereas this difference does not exceed 0.02 Å for other bonds, which often fall within the 3σ interval of the experimental data.

In the ground states of complexes **1′** ($S=3$) and **2′** ($S=3/2$) and in the BS state of **1′**, the spin density is localized mostly at the metal atoms (2.73–2.74 e) with small contributions coming from the Cl and N atoms (up to 0.09 e; Figure 4, Table 3). Nevertheless, the spin density at the Co atoms is lower than expected for the ideal case of d^7 Co^{II} centers, and this reflects some spin delocalization between Co and the donor Cl and N atoms.

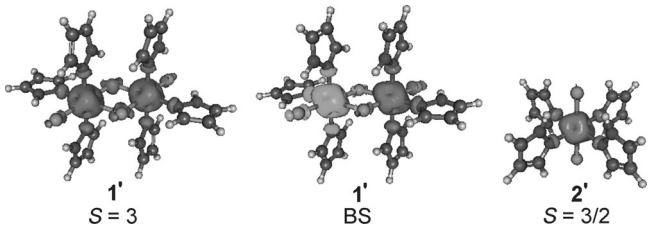

Figure 4. Spin density distribution in **1′** and **2′**.

Oxidized Complexes

The single-point calculation of oxidized species $\mathbf{2'}^{+}$ performed on the basis of the equilibrium geometry of **2′** shows that the quintet configuration $S=2$ is the ground state of $\mathbf{2'}^{+}$, with unrelaxed geometry (denoted as $\{\mathbf{2'}^{+}\}$) being 3.3 kcal mol^{-1} lower in energy than the singlet state. The total spin density at the Co atom increases from 2.73 to only 2.99 e on going from **2′** to $\{\mathbf{2'}^{+}\}$, and the total spin densities at the Cl and donor N atoms increase from 0.04–0.05 to 0.12–0.20 e (Table 3). Such spin-density distribution corresponds to that expected for the free d^7 Co^{II} center bearing three unpaired electrons and indicates that the Co atom preserves its II+ oxidation state upon vertical oxidation of **2′**. Thus, the oxidation of **2′** at the initial moment (i.e., before geometry relaxation) affects mostly the chloride and pyrazolyl ligands, whereas the involvement of the metal atom is rather insignificant.

Full geometry optimization of $\mathbf{2'}^{+}$ resulted in a change in the relative stability of the spin states; the singlet configuration corresponding to the d^6 Co^{III} low-spin complex became the ground state for the optimized structure of $\mathbf{2'}^{+}$, whereas the high-spin quintet state $S=2$ was 17.1 kcal mol^{-1} higher in energy. Thus, the Co^{II}/Co^{III} oxidation occurs mostly at the latter stage (during geometry relaxation) as a result of the intramolecular redox process. Geometry optimization of $\mathbf{2'}^{+}$ did not result in a significant alteration in the molecular structure, which led to shortening of the Co–Cl and Co–N bonds (by 0.309 and 0.163 Å, respectively, for the low-spin state).

Energies of dinuclear monooxidized species $\mathbf{1'}^{+}$ with unrelaxed geometry ($\{\mathbf{1'}^{+}\}$) are similar for the octet ($S=7/2$), sextet ($S=5/2$), and BS spin configurations; the first is more stable than the others only by 0.6 kcal mol^{-1}. Other spin states (including that with $S=3/2$) have clearly higher energies. The ground state of unoptimized dioxidized complex $\{\mathbf{1'}^{2+}\}$ is nonet ($S=4$). For both $\{\mathbf{1'}^{+}\}$ and $\{\mathbf{1'}^{2+}\}$, the spin density at the Co atoms does not exceed 3 e, whereas that at the Cl and N atoms reaches 0.16–0.24 e (Table 3), which indicates that the vertical single and double electron oxidations of **1′** (e.g., those occurring at very fast scan rate) mostly involve the ligands rather than the metal atoms.

Similarly to the case of mononuclear complex $\mathbf{2'}^{+}$, full geometry optimization changed the ground states of the oxidized binuclear species. The quartet state of $\mathbf{1'}^{+}$ ($S=3/2$) has the lowest energy, whereas the octet ($S=7/2$) and sextet ($S=5/2$) states are 12.2 and 11.0 kcal mol^{-1} higher in energy. The spin density in the ground state of $\mathbf{1'}^{+}$ is almost completely localized at one of the $\{CoCl(pyr)_3\}^{+}$ fragments (2.73 e at the Co atom, Table 3), whereas another fragment is in fact the closed-shell one. Such spin density distribution corresponds to the oxidation of only one Co atom during the $\mathbf{1'}\rightarrow\mathbf{1'}^{+}$ process.

Finally, the ground state of optimized doubly oxidized complex $\mathbf{1'}^{2+}$ is the closed shell singlet, which is typical for the low-spin d^6 Co^{III} configuration of both metal centers. The septet, nonet, and BS configurations are higher in energy by 19.3, 23.3, and 23.6 kcal mol^{-1}, respectively. Thus,

Table 3. Calculated atomic spin densities [e].[a]

Atom	**1′** $S=3$	**1′** BS	$\{\mathbf{1'}^{+}\}$ $S=7/2$	$\mathbf{1'}^{+}$ $S=3/2$	$\{\mathbf{1'}^{2+}\}$ $S=4$	$\{\mathbf{1'}^{-}\}$ $S=5/2$	$\{\mathbf{1'}^{2-}\}$ $S=2$	**2′** $S=3/2$	$\{\mathbf{2'}^{+}\}$ $S=2$	$\{\mathbf{2'}^{-}\}$ $S=1$
Co1	2.74	2.73	2.93	2.73	2.94	2.40	2.24	2.73	2.99	2.03
Cl1	0.09	0.01	0.19	0.03	0.22	0.07	0.07	0.05	0.20	0.02
Cl2	0.06	0.06	0.18	0.07	0.24	0.03	0.02	0.05	0.20	0.02
N_M[b]	0.03–0.04	0.03–0.04	0.08–0.10	0.31–0.47	0.12–0.16	0.02–0.03	0.02	0.04	0.12	0.02
N_{nM}[c]	0.00	0.00	0.00–(−0.01)	0.00	−0.01	0.00	−0.01	0.00	−0.01	−0.01
$Co1^{i}$	2.74	−2.73	2.79	0.00	2.94	2.35	1.55			
$Cl1^{i}$	0.09	−0.01	0.23	0.02	0.22	0.07	0.07			
$Cl2^{i}$	0.06	−0.06	0.16	0.00	0.24	0.03	0.04			
$N_M{}^{i}$[b]	0.03–0.04	(−0.03)–(−0.04)	0.04–0.06	0.00	0.12–0.16	0.02–0.03	0.03			
$N_{nM}{}^{i}$[c]	0.00	0.00	0.00	0.00	−0.01	0.00–(−0.01)	0.00			

[a] See Figures 1 and 2 for atomic numbering. [b] Metal-bound atoms. [c] Atoms that are not bound to the metal.

the single or double electron oxidations of **1′** are metal centered at a sufficiently slow scan rate which allows geometry relaxation.

Reduced Complexes

The ground state of reduced complex $\{\mathbf{2'}^{-}\}$ with unrelaxed geometry is triplet ($S=1$). The spin density value at the Co atom in $\{\mathbf{2'}^{-}\}$ (2.03 e, Table 3) is typical for the octahedral d^8 configuration (Co^{I} center). Geometry optimization of $\mathbf{2'}^{-}$ resulted in cleavage of both Co–Cl bonds, elimination of two Cl^- ligands to the second coordination sphere, and tetrahedral distortion of the coordination polyhedron. These results are in agreement with the irreversible character of the reduction waves for the complexes under study.

A similar effect was also found for the vertical single electron reduction of **1′** to $\{\mathbf{1'}^{-}\}$ ($S=5/2$), that is, the spin density at both Co atoms decreased from 2.74 to 2.35–2.40 e, whereas that at the other atoms changed insignificantly (Table 3). Finally, the spin density values at the Co centers in the unrelaxed doubly reduced complex $\{\mathbf{1'}^{2-}\}$ ($S=2$) are not equal. However, they indicate that both single and double electron reductions of **1′** are mostly metal centered. Geometry optimization of $\mathbf{1'}^{-}$ and $\mathbf{1'}^{2-}$ also led to decomposition of these complexes.

Oxidation of Cyclohexane to Cyclohexanol and Cyclohexanone

The complexes act as catalyst precursors for peroxidative oxidation, in NCMe/H_2O, by aqueous H_2O_2 (in a slightly acidic medium, at room temperature and under an atmosphere of nitrogen), of cyclohexane to cyclohexanol (main product) and cyclohexanone, according to the overall reaction outlined in Equation (1). In fact, after 6 h, complex **1** exhibits overall turnover numbers (TONs) up to 223 moles of products per mole of catalyst (Table 4). This value is considerably higher than those presented by related Cu[3g,k] and V[3f,k] complexes, similar to Re,[3j] but lower than Fe[3c,k] C-scorpionate complexes.

Cyclohexane oxidation by hydrogen peroxide did not take place in the absence of the metal complex or the oxidant. The Co complexes acted more efficiently in the presence of nitric acid, as previously described for other systems,[3f,k,l,15] as it activates the catalyst by ligand protonation (to yield 3-phenylpyrazolium) with resulting promotion of the unsaturation of the metal and by enhancement of its oxidative properties. The acid can also hamper the decomposition of the peroxide and stabilize intermediate peroxo species.[15j]

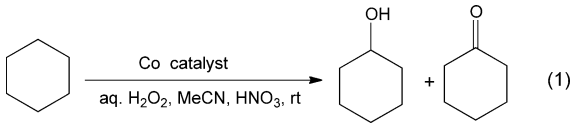

(1)

By taking into consideration the number of Co atoms per molecule of catalyst precursor, their order of activity in terms of maximum TON per metal is as follows: $[CoCl_2(H_2O)\{CH_3SO_2OCH_2C(pz)_3\}]$ (**7**), $[Co(OSO_3H)(OCH_3)(HOCH_3)\{HC(pz)_3\}]$ (**3**), $[CoCl(\mu\text{-}Cl)(Hpz^{Ph})_3]_2$ (**1**), $[CoCl_2(Hpz^{Ph})_4]$ (**2**), $[Co\{HOCH_2C(pz)_3\}_2](NO_3)_2$ (**4**), $[Co\{HOCH_2C(pz)_3\}_2][Co\{HOCH_2C(pz)_3\}(H_2O)_3]_2(Cl)_6{\cdot}6H_2O$ (**5**), and $[CoCl_2(H_2O)\{PyCH_2OCH_2C(pz)_3\}]$ (**6**) with TONs/Co of 209, 142, 112, 105, 94, 65, and 64, respectively.

The catalytic activities of our complexes are much higher than that of the $CoCl_2$ salt under the same experimental conditions (Table 4, entry 29 versus entries 4, 8, 12, 16, 20, 24, and 28).

Table 4. Peroxidative oxidation of cyclohexane to cyclohexanol and cyclohexanone catalyzed by compounds **1–7**.[a]

Entry	Catalyst	$n(H_2O_2)/n(cat)\times10^{-3}$	$n(cat)/n(C_6H_{12})\times10^{5}$	TON[b]		
				Cyclohexanol	Cyclohexanone	Total[c]
1	**1**	1	200	1.0	0.2	1.2
2	**1**	2	100	6.2	1.9	8.1
3	**1**	20	10	50.2	27.4	77.6
4	**1**	40	5	160	62.8	223
5	**2**	1	200	0.3	0.6	0.9
6	**2**	2	100	5.8	0.9	6.7
7	**2**	20	10	26.7	17.1	43.8
8	**2**	40	5	60.2	44.6	105
9	**3**	1	200	0.9	0.3	1.2
10	**3**	2	100	3.4	2.1	5.5
11	**3**	20	10	66.2	27.1	93.3
12	**3**	40	5	95.4	46.8	142
13	**4**	1	200	0.4	0.2	0.6
14	**4**	2	100	5.2	2.2	7.4
15	**4**	20	10	42.0	25.0	67.0
16	**4**	40	5	56.7	37.6	94.3
17	**5**	1	200	3.9	9.0	12.9
18	**5**	2	100	6.4	5.0	11.4
19	**5**	20	10	60.5	5.4	65.9
20	**5**	40	5	187	7.7	195
21	**6**	1	200	0.3	0.2	0.5
22	**6**	2	100	1.4	1.9	3.3
23	**6**	20	10	9.7	12.7	22.4
24	**6**	40	5	24.8	39.2	64.0
25	**7**	1	200	2.0	0.9	2.9
26	**7**	2	100	5.1	4.7	9.8
27	**7**	20	10	39.8	49.9	89.7
28	**7**	40	5	104	105	209
29	$CoCl_2$	40	5	4	6	10

[a] Reaction conditions: C_6H_{12} (5 mmol), NCMe (3.0 mL), $n(H_2O_2)/n(C_6H_{12})=1$, $n(HNO_3)/n(\text{catalyst})=10$, 20 °C, 6 h. [b] Turnover number (moles of product per mol of catalyst); yield [%] can be estimated as $TON\times[n(\text{catalyst})/n(C_6H_{12})]\times100$. [c] Cyclohexanol + cyclohexanone.

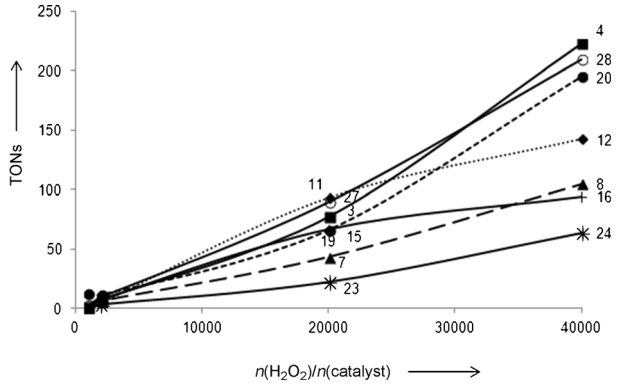

Figure 5. Effect of the amount of H_2O_2 (H_2O_2/catalyst molar ratio) on the overall TON by using as catalyst precursor $[CoCl(\mu\text{-}Cl)(Hpz^{Ph})_3]_2$ (**1**) (■), $[CoCl_2(Hpz^{Ph})_4]$ (**2**) (▲), $[Co(OSO_3H)(OCH_3)(HOCH_3)\{HC(pz)_3\}]$ (**3**) (◆), $[Co\{HOCH_2C(pz)_3\}_2](NO_3)_2$ (**4**) (+), $[Co\{HOCH_2C(pz)_3\}_2][Co\{HOCH_2C(pz)_3\}(H_2O)_3]_2(Cl)_6{\cdot}6H_2O$ (**5**) (●), $[CoCl_2(H_2O)\{PyCH_2OCH_2C(pz)_3\}]$ (**6**) (*), and $[CoCl_2(H_2O)\{CH_3SO_2OCH_2C(pz)_3\}]$ (**7**) (○). Reaction conditions and point numbers are those of Table 4.

The influence of the amount of hydrogen peroxide on the catalytic activity was investigated and shown to have a pronounced effect (Table 4, Figure 5): the overall TON increased from 1.2 (for **1**), 0.9 (for **2**), 1.2 (for **3**), 0.6 (for **4**), 12.9 (for **5**), 0.5 (for **6**), and 2.9 (for **7**), to 223, 105, 142, 94, 195, 64, and 209, respectively, upon changing the oxidant/catalyst molar ratio from 1×10^3 to 40×10^3 (Table 4).

Although the detailed mechanisms of the reactions are unknown, we believe they proceed by means of a radical pathway involving both C- and O-centered radicals, because, as observed in other cases,[3c,f,g,k,l] the formation of the cyclohexanol and cyclohexanone products is nearly suppressed if the reactions that correspond to the highest activity for complex **6** are performed in the presence of a radical trap for carbon (such as trichlorobromomethane, $CBrCl_3$), in a stoichiometric amount relative to the substrate, or in the presence of a radical trap for oxygen (such as diphenylamine, Ph_2NH), in a stoichiometric amount relative to H_2O_2.

The presence of cyclohexylhydroperoxide (CyOOH) at the end of the reaction (under the conditions of Table 4) is shown by the increase in the amount of cyclohexanol with a corresponding decrease in that of cyclohexanone, upon treatment of the final reaction solution with an excess amount of PPh_3 prior to GC analysis, according to the method reported by Shul'pin.[16] Reduction of CyOOH by PPh_3 gives cyclohexanol (with formation of phosphane oxide), which thus replaces the decomposition of CyOOH to both cyclohexanol and cyclohexanone in the gas chromatograph.

Hence, the oxidation of cyclohexane (CyH) could proceed as follows. Metal-assisted decomposition of H_2O_2 could lead to the hydroxyl radical ($HO^{\cdot}$), which upon H abstraction from cyclohexane (CyH) would form the cyclohexyl radical ($Cy^{\cdot}$).[16–18] The formation of the $HO^{\cdot}$ radical should involve both Co^{3+} (see XAS studies, below) and Co^{2+} redox states (the former leading to H_2O_2 oxidation to $HOO^{\cdot}$ and the latter to H_2O_2 reduction with liberation of $HO^{\cdot}$), as well as proton-transfer steps among H_2O_2, hydroperoxo, and peroxo metal species, similarly to what has been indicated[16–18] for some $V^{5+/4+}$, $Re^{7+/6+}$, and $Cu^{2+/}Cu^{+}$ catalysts. Such H^+ shifts are expected to be catalyzed by water.[17a,18]

Upon reaction with O_2 or with a metal-peroxo intermediate species, that is, [Co]-OOH, the cyclohexyl radical could form $CyOO^{\cdot}$ (peroxyl radical) or CyOOH, respectively. $CyOO^{\cdot}$ can also form CyOOH upon H abstraction from H_2O_2,[16–18] and CyOOH can decompose into the final products (cyclohexanol CyOH and cyclohexanone). Moreover, Co^{3+}- or Co^{2+}-promoted decomposition of CyOOH could lead to the peroxyl ($CyOO^{\cdot}$) or oxyl ($CyO^{\cdot}$) radical, respectively, and CyOH could then be formed by H abstraction from cyclohexane by $CyO^{\cdot}$ or upon decomposition of $CyOO^{\cdot}$ to both cyclohexanol (CyOH) and cyclohexanone.[16–18]

The catalytic activity (overall TON) increased with a decrease in the oxidation potential (easier Co^{2+} oxidation) for complexes **1**–**3**, but such a trend was not followed by **4**–**6** possessing a basic substituent at the scorpionate ligand, as they displayed lower activity than that expected in terms of that correlation, whereas complex **7**, with a labile water ligand and without such a basic substituent, was more active than expected. Hence, other factors (e.g., basic properties of ligands and their lability), apart from the redox potential, also have to be taken into account.

X-ray Absorption Spectroscopy (XAS)

X-ray absorption near-edge structure (XANES) is very sensitive to the oxidation state and local symmetry of the absorbing atoms.[19] Figure 6a shows the XANES spectra for complexes **1** and **2** starting catalyst precursors. Both complexes display a weak pre-edge feature at approximately 7709 eV that can be assigned to the 1s→3d transition.[20] The pre-edge position can be used to indicate the oxidation state of absorbing atom. The pre-edge positions for both complexes are the same with the Co^{2+} reference, and the oxidation states of the Co ions is 2+ for both of them. The intensity of the 1s→3d absorption band is sensitive to the symmetry around the absorption atoms, and this band has been observed as a characteristic feature for cobalt compounds with octahedral symmetry. This confirms that both complexes display this type of geometry. However, the XANES features of both complexes are different, which indicates that their Co environments are dissimilar.

After hydrogen peroxide (H_2O_2) was added into solutions of complexes **1** and **2**, the XANES spectra features were altered and became almost the same for both complexes, in what concerns XANES features and intensities in the solvent environment. This demonstrates that the local symmetry around the Co ions become almost the same for both complexes in solution, upon addition of H_2O_2. Moreover, the pre-edge positions become the same as that of Co^{3+} reference; this indicates that the oxidation state in derived species Ox-**1** and Ox-**2** (from complexes **1** and **2**, in this order) is +3. This similarity is in accord with the theoretical studies

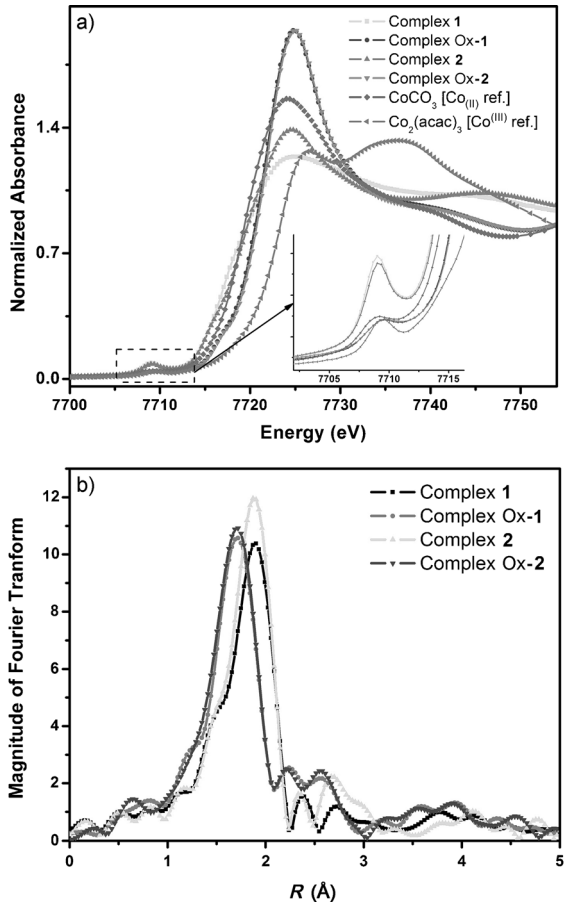

Figure 6. a) Co K-edge XANES spectra for complexes **1** and **2** and for species Ox-**1** and Ox-**2**; b) Fourier transform of Co K-edge EXAFS spectra for complexes **1** and **2** obtained before and after adding hydrogen peroxide as the oxidant.

(see above), and this suggests that the dimeric structure of complex **1** converts easily into a mononuclear one. The XANES observations suggest that the oxidized metal species in the peroxidative oxidation of cyclohexane obtained from complexes **1** and **2** (Ox-**1** and Ox-**2**, respectively) are nearly the same.

The Fourier transform (FT) spectra for all complexes are shown in Figure 6b. The band intensity is sensitive to the number and type of atoms coordinated to the absorbing atom, and as seen for **1** and **2**, the detected difference in band intensity is indicative of dissimilarities in the local environment around the respective Co centers, which is consistent with the XANES observation. After adding the H_2O_2 oxidant, the band intensities for oxidized complexes Ox-**1** and Ox-**2** are nearly the same, and this suggests analogous metal environments. Moreover, for the latter species the band positions are shifted to lower distances relative to those of **1** and **2**, which can be ascribed to the higher oxidation state of the metal cations with subsequent stronger and shorter bonds. Hence, XAS characterization suggests that species Ox-**1** and Ox-**2** in the oxidation of cyclohexane, derived from oxidation of **1** and **2**, respectively, are essentially the same. Such a species, under the used mild reaction conditions, does not undergo significant structural alterations for a period of 6 h (Figure S2). However, various attempts to isolate and fully characterize it were unsuccessful.

Cell Cytotoxicity of the Compounds

Viability assays of water-soluble **2** were evaluated in vitro by the MTS metabolism assay [MTS = 3-(4,5-dimethylthiazol-2-yl)-5-(3-carboxymethoxyphenyl)-2-(4-sulfophenyl)-2*H*-tetrazolium] in human colorectal carcinoma (HCT116) and breast adenocarcinoma (MCF7) cell lines and in normal human fibroblasts (Figure 7).

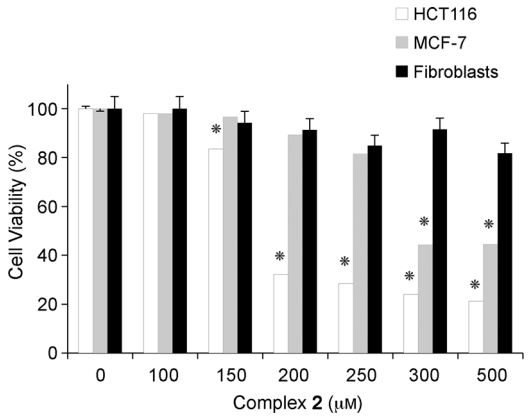

Figure 7. Effect of complex **2** exposure on HCT116, MCF7, and normal fibroblasts cell viability. Cells were exposed to complex **2** (0–500 μM) or water (vehicle control, 0 μM of complex) for 48 h. The results are expressed as mean ±SEM fold-change compared to controls from at least three independent experiments. The symbol * in the figure implies that the results are statistically significant with $p < 0.01$ (as compared to control for each compound and cell line).

Our results demonstrated that a 200 μM concentration of complex **2** decreased HCT116 cell viability to 32% compared to control cells ($p < 0.01$, Figure 7). In addition, a similar concentration of this complex decreased breast MCF7 cell viability to 89% ($p < 0.05$, Figure 7). In this regard, complex **2** cytotoxicity is higher for the HCT116 tumor cell line [$IC_{50} = (169.6 \pm 5.3)$ μM] than for the MCF7 tumor cell line [$IC_{50} = (285.2 \pm 3.7)$ μM, Figure 7]. Our previous results obtained by using cobalt complexes **5**, **6**, and **7** demonstrated moderate cytotoxic potential.[4] Indeed, complexes **2** and **5** were the most effective ones in reducing cell viability (Figure 7 and Ref. [4]). Complex **2** presented much higher IC_{50} values for the HCT116 and MCF7 tumor cells than the common antitumor drugs cisplatin (4.14 μM)[21] and doxorubicin (1.4 μM).[22] The antiproliferative activity of complex **2** was also accessed in melanoma (MNT1) and hepatocellular (HepG2) cell lines, and the IC_{50} values were higher than 500 μM (results not shown); this indicates that they are ineffective in those cell lines.

To gain insight into the effect of complex **2** in nontumoral cells, MTS assays were also performed in normal (non-ma-

lignant) human fibroblasts (Figure 7). For the highest concentration tested for this complex (500 μM) there were still 81.8% of viable cells (Figure 7). Indeed, at the concentration corresponding to the IC_{50} for the HCT116 tumor cell line there were 94.2% of viable fibroblasts. Although HCT116 and MCF7 are epithelial types of tumor cells, this result is very promising, and viability assays will also be performed in normal epithelial cell lines to confirm the higher cytotoxicity of complex **2** in the colorectal carcinoma cell line.

The search for correlations of the redox potential with cytotoxicity has been a subject of current interest,[23] but the Co compounds of this study do not appear to follow any clear relation, which is not unexpected in view of the fact that they present the metal already with the known[24] active oxidation state (2+).

Conclusions

We were able to prepare novel 3-phenylpyrazol Co^{II} complexes either through $C(sp^3)$–N(pyrazolyl) bond cleavage at $HC(pz^{Ph})_3$ (**1**) or by direct reaction with Hpz^{Ph} (**2**). Thus, this study contributes toward the development of the still little explored coordination chemistry of such types of pyrazole-based ligands.

The work also opened up the possibility of applying such a type of complex as a catalyst precursor for the single-pot oxidation of cyclohexane to cyclohexanol and cyclohexanone under mild conditions at room temperature and with an environmentally friendly oxidant (i.e., H_2O_2).

The mononuclear complex $[CoCl_2(H_2O)\{CH_3SO_2OCH_2C(pz)_3\}]$ (**7**), which bears a methylsulfonate C-functionalized scorpionate and a labile water ligand, was responsible for the best catalytic activity per cobalt atom, which in a slightly acidic medium corresponds to a TON up to approximately 210. The pyridyl-substituted scorpionate complex $[CoCl_2(H_2O)\{PyCH_2OCH_2C(pz)_3\}]$ (**6**) and those (i.e., **4** and **5**) with the hydroxy-substituted one are less active per cobalt atom. This could suggest that a nonbasic substituent at the scorpionate has a more favorable effect than a basic one, but further studies with a wider variety of substituted scorpionate complexes will be required to confirm this hypothesis.

Theoretical calculations at the DFT level of theory demonstrated that the vertical oxidation of **1** and **2**, that is, the oxidation at the initial moment before the structural relaxation, affects mostly the chloride and pyrazolyl ligands, whereas the adiabatic oxidation (that after the geometry relaxation), as well as the reduction, are mostly metal centered. Therefore, interestingly, the metal oxidation occurs by intramolecular electron-transfer at the initially ligand-centered oxidized species.

In situ XAS study showed that the addition of hydrogen peroxide as an oxidant to a solution of complexes **1** and **2** caused a change in the oxidation state of cobalt from +2 to +3 and resulted in a common Co^{+3} species that does not undergo considerable structural changes along the reaction under the applied mild reaction conditions. The catalytic activity of the Co^{2+} complexes tended to increase as the oxidation potential was decreased (easier oxidation), and this is in accord with the relevance of oxidized Co^{3+} species and also with the absence of a basic substituent at the methine C atom of the scorpionate ligand.

The cytotoxicity of complex **2** toward the colorectal HCT116 tumor cell line [$IC_{50} = (169.6 \pm 5.3)$ μM] was higher than its cytotoxicity toward the breast MCF-7 tumor cell line [$IC_{50} = (285.2 \pm 3.7)$ μM]. Despite that, these in vitro antiproliferative activities are much lower than that exhibited by cisplatin.[21] However, complex **2** showed a very low cytotoxicity in the normal (nonmalignant) human fibroblast cell line ($IC_{50} > 500$ μM), which may be considered a positive feature for further development. No clear relationship was observed between the oxidation potential and the bioactivity, and this substantiates the bioactive 2+ oxidation state for cobalt compounds.

Experimental Section

General Materials and Procedures

3-Phenyl-1*H*-pyrazole, sulfur trioxide trimethylamine complex (Aldrich), cobalt(II) chloride, hydrogen peroxide (30%, Fluka), acetonitrile, diethyl ether, chloroform, nitric acid (65%), cycloheptanone (Riedel-de-Haën), methanol (Lab-Scan), and cyclohexane and triphenylphosphine (Merck) were used as received from the supplier. $HC(pz^{Ph})_3$,[3g] $[Co(OSO_3H)(OCH_3)(HOCH_3)\{HC(pz)_3\}]$ (**3**), $[Co\{HOCH_2C(pz)_3\}_2](NO_3)_2$ (**4**), $[Co\{HOCH_2C(pz)_3\}_2][Co\{HOCH_2C(pz)_3\}(H_2O)_3]_2(Cl)_6{\cdot}6H_2O$ (**5**), $[CoCl_2(H_2O)\{PyCH_2OCH_2C(pz)_3\}]$ (**6**), and $[CoCl_2(H_2O)\{CH_3SO_2OCH_2C(pz)_3\}]$ (**7**) were obtained according to published methods.[4]

Infrared (IR) spectra (4000–400 cm^{-1}) were recorded with a Bio-Rad FTS3000MX in KBr pellets; wavenumbers are in cm^{-1}; abbreviations: vs., very strong; s, strong; m, medium; w, weak. Far-infrared spectra (FIR, 400–200 cm^{-1}) were recorded with a Vertex 70 spectrophotometer in CsI pellets.

ESI+/ESI− mass spectra were obtained with a Varian 500-MS LC ion trap mass spectrometer [solvent = MeOH, flow = 20 μL min^{-1}, needle spray voltage = ±5 kV, capillarity voltage = ±100 V, nebulizer gas (N_2) = 35 psi, drying gas (N_2) = 10 psi; drying gas temperature (N_2) = 350 °C; 1 psi = 6.89 kPa]. For the MS spectra description, *M* denotes the complex part of **1** and **2**.

C, H, and N elemental analyses were performed by the Micro Analytical Service of the Instituto Superior Técnico.

The electrochemical experiments were performed with an EG&G PAR 273A potentiostat/galvanostat connected to a personal computer through a GPIB interface. Cyclic voltammograms were obtained in 0.2 M [nBu_4N][BF_4]/NCMe at a platinum disc working electrode ($d = 1$ mm). Controlled-potential electrolyses (CPE) were performed in electrolyte solutions with the above-mentioned composition in a three-electrode H-type cell. The compartments were separated by a sintered glass frit and equipped with platinum gauze working and counter electrodes. For both CV and CPE experiments, a Luggin capillary connected to a silver wire pseudoreference electrode was used to control the working electrode potential. The CPE experiments were monitored regularly by CV; this assured no significant potential drift occurred along the electrolyses. Ferrocene was used as an internal standard for the measurement of the oxidation potentials of the complexes; the redox potential values are quoted relative to the SCE by using as internal reference the ferrocene/ferrocenium ($[Fe(\eta^5\text{-}C_5H_5)_2]^{0/+}$) couple ($E^{ox}_{1/2} = 0.42$ V vs. SCE in NCMe).[25]

Gas chromatographic (GC) measurements were performed by using a FISONS Instruments GC 8000 series gas chromatograph with a flame ionization detector (FID) and a capillary column (DB-WAX, column length: 30 m; internal diameter: 0.32 mm). The temperature of the injector was of 240 °C. The initial temperature was maintained at 100 °C for 1 min then raised 10 °C min^{-1} to 180 °C and held at that temperature for 1 min. Helium was used as the carrier gas.

GC–MS analysis was performed by using a Clarus 600 PerkinElmer. The ionization voltage was 70 eV. Gas chromatography was conducted in the temperature-programming mode by using a SGE BPX5 column (30 m × 0.25 mm × 0.25 μm). Reaction products were identified by comparison of their retention times with known reference compounds and by comparing their mass spectra to fragmentation patterns obtained from the NIST spectral library stored in the computer software of the mass spectrometer.

X-ray Absorption Spectroscopy (XAS) Measurements

XAS measurements were performed at the beam line BL07A1 of the National Synchrotron Radiation Research Center (NSRRC) at Hsinchu, Taiwan. The storage ring of the electron accelerator had energy of 1.5 GeV and an operation current of 360 mA. A Si(111) double crystal monochromator was used to perform energy scan, of which the parallelism can be adjusted to eliminate the high-order harmonics. All XAS spectra were recorded by using the fluorescence detection mode. Samples were mounted at a 45° angle to the beam to collect fluorescence spectra with best data quality. The intensity of the incident beam was measured with a He/N_2-filled ionization chamber installed in front of the sample. Fluorescence from the sample was recorded by using an Ar-filled Lytle detector and the characteristic $CoK_{\alpha 1}$ fluorescence signal was removed by a Fe filter. The absorption coefficient was calculated from the intensity ratio of the fluorescence and incident beams. The references Co metal foils were measured simultaneously as a standard for energy calibration in each scan. The beam size was limited by the horizontal and vertical slits with the area of 2 × 2 mm^2 during XAS measurements.

X-ray Crystal Structure Determinations

The X-ray diffraction data of **1** and **2** were collected by using a Bruker AXS-KAPPA APEX II diffractometer with graphite monochromated MoK_{α} radiation. Data were collected at 293 (for **1**) or 150 (for **2**) K by using Ω scans of 0.5° per frame, and a full sphere of data was obtained. Cell parameters were retrieved by using Bruker SMART software and refined by using Bruker SAINT on all the observed reflections. Absorption corrections were applied by using SADABS.[26a] Structures were solved by direct methods by using the SHELXS-97 package and refined with SHELXL-97.[26b] Calculations were performed by using the WinGX System Version 1.80.03.[26c] Hydrogen atoms were inserted in calculated positions. Least-square refinement with anisotropic thermal motion parameters for all non-hydrogen atoms and isotropic for the remaining atoms gave $R1 = 0.0788$ (for **1**) or 0.0445 (for **2**) [$I > 2\_(I)$; $R1$ (all data) = 0.1650 (for **1**) or 0.1189 (for **2**)]. The maximum and minimum bands in the final difference electron density map were of 0.669 and −0.452 (for **1**) or 0.372 and −0.570 (for **2**). CCDC-931714 (for **1**) and -931715 (for **2**) contain the supplementary crystallographic data for this paper. These data can be obtained free of charge from The Cambridge Crystallographic Data Centre via http://www.ccdc.cam.ac.uk/data_request/cif.

Computational Details

Full geometry optimization of the complexes was performed in Cartesian coordinates at the DFT/HF hybrid level of theory by using Becke's three-parameter exchange functional[27a] in combination with the gradient-corrected correlation functional of Lee, Yang, and Parr[27b] (UB3LYP) with the help of the Gaussian 09[28] program package. The broken-symmetry (BS) approach[29a–c] was applied with the Gaussian keyword Guess = mix. The experimental X-ray structures of **1** and **2** (this work) were taken as a basis for the initial geometries of the optimization processes. Symmetry operations were not applied for all structures. A relativistic Stuttgart pseudopotential describing 10 core electrons and the corresponding basis set[30] for the cobalt atom and the 6-31G(d) basis set for other atoms were used. The Hessian matrix was calculated analytically to prove the location of correct minima (no imaginary frequencies were found). Solutions with stable wavefunctions were achieved for all structures by using the Gaussian keyword Stable(Opt). The magnetic coupling parameter J was calculated for **1′** by using Equations (2)[29d–f] and (3):[29g]

$$J = \frac{E(\mathrm{LS}) - E(\mathrm{HS})}{S^2_{\max}} \quad (2)$$

$$J = \frac{E(\mathrm{LS}) - E(\mathrm{HS})}{<S^2>(\mathrm{HS}) - <S^2>(\mathrm{LS})} \quad (3)$$

in which E(LS) and E(HS) are energies of the low-spin and high-spin states, $S_{\max}$ is the spin size for the high-spin state, and $<S^2>$(HS) and $<S^2>$(LS) are the total spin angular momentum for the high-spin and low-spin states, respectively.

Cell Culture

HCT116 human colorectal carcinoma, MCF7 breast adenocarcinoma cell lines, and normal human fibroblasts were grown as previously described.[31]

Synthesis and characterization of the complexes

$[CoCl(\mu\text{-}Cl)(Hpz^{Ph})_3]_2$ (**1**): $HC(pz^{Ph})_3$ (0.81 g, 1.54 mmol) in MeOH (10 mL) was added to a solution of cobalt chloride (0.20 g, 1.54 mmol) in MeOH (30 mL) with constant stirring in air. The resulting pink solution was stirred overnight and then concentrated. Upon the addition of Et_2O, a pink solid precipitated. It was collected by filtration, washed with Et_2O, and dried in vacuo (1.08 g, 62 %). Compound **1** is soluble in MeOH, NCMe ($S_{25\,°C} \approx 5.0$ mg mL^{-1}), CH_2Cl_2, and acetone. Suitable crystals for X-ray analyses were obtained upon slow diffusion of Et_2O into a methanol solution of the complex. IR (KBr pellet): $\tilde{\nu} = 1530$, 1497 [s, ν(C=C) and ν(N=C), Hpz^{Ph}]; 1182, 1119, 1100 cm^{-1} [s, Hpz^{Ph}]. FIR (CsI pellet): $\tilde{\nu} = 312$, 275 cm^{-1} [m, ν(Co-Cl)]. MS (ESI+): m/z: 1089 ($[M-Cl]^+$), 527 ($[M-2Cl]^{2+}$). Elemental analysis calcd (%) for $C_{54}H_{48}Cl_4Co_2N_{12}{\cdot}0.75Et_2O$ (1180.31): C 58.0, H 4.7, N 14.2; found: C 58.3, H 4.4, N 14.5.

$[CoCl_2(Hpz^{Ph})_4]$ (**2**): Hpz^{Ph} in a 1:4 molar ratio (1.76 g, 3.08 mmol) in MeOH (30 mL) was added to a solution of $CoCl_2$ (0.10 g, 0.77 mmol) in MeOH (20 mL) with constant stirring. The resulting pink solution was stirred overnight and then concentrated. Upon the addition of Et_2O, a pink solid precipitated. The solid was collected by filtration, washed with Et_2O, and dried in vacuo (0.28 g, 52 %). Compound **2** is soluble in NCMe ($S_{25\,°C} \approx 4.6$ mg mL^{-1}), H_2O, MeOH, CH_2Cl_2, and acetone. Crystals suitable for X-ray diffraction were obtained by diffusion of Et_2O into a methanol solution of the complex. IR (KBr pellet): $\tilde{\nu} = 1568$, 1469 cm^{-1} [s, ν(N=C), (N=N), Hpz^{Ph}]. FIR (CsI pellet): $\tilde{\nu} = 245$, 230 cm^{-1} [m, ν(Co-Cl)]. MS (ESI+): m/z: 671 ($[M-Cl]^+$), 527 ($[M-Cl-Hpz^{Ph}]^+$), 382 ($[M-Cl-2Hpz^{Ph}]^+$). Elemental analysis calcd (%) for $C_{36}H_{32}Cl_2CoN_8$ (706.53): C 61.2, H 4.6, N 15.9; found: C 61.2, H 4.6, N 16.0.

Catalytic Activity Studies

The oxidation reactions were performed in Schlenk tubes. Under typical conditions, the reaction mixtures were prepared as follows: catalyst precursor **1–7** (0.010 mmol) was dissolved in NCMe (2.00 mL). The required amount of this solution for the desired oxidant/catalyst molar ratio was transferred to a second flask, into which NCMe was added to a total solution volume of 3.00 mL. H_2O_2 (30 % in H_2O, 0.50 mL, 5.00 mmol) and cyclohexane (0.54 mL, 5.00 mmol) were then added (in this order), and the reaction solution was stirred for 6 h at the desired temperature (commonly room temperature) and normal pressure. In the experiments with HNO_3, this acid was added immediately before the addition of the substrate. In the experiments without the addition of NCMe, this solvent was replaced by the same amount of water.

For product analysis, cycloheptanone (internal standard, 90 μL) and diethyl ether (to extract the substrate and the organic products from the reaction mixture, 5.0 mL) were added. The obtained mixture was stirred for 10 min and then a sample (1 μL) was taken from the organic phase

and analyzed by GC by the internal standard method. Blank experiments confirmed that no cyclohexanol or cyclohexanone was formed without the metal catalyst. The presence of cyclohexylhydroperoxide was checked upon the addition of PPh_3 to the final reaction according to the method reported by Shul'pin[16] and applied to various catalytic systems.[16–18]

EXAFS Studies

The EXAFS studies were performed in a designed in situ cell. Complex **1** (0.0600 g, 5.3×10^{-5} mol) or complex **2** (0.0466 g, 6.6×10^{-5} mol) was dissolved in NCMe (10.0 mL), and 30% H_2O_2 (3.3 mL) and 65% HNO_3 (0.3 mL) were added to the above solution. Then, cyclohexane (1.78 mL) was added, and the system was stirred for 1 h. The reaction was monitored for 6 h, and the XAS spectrum was acquired every hour.

Standard procedures were followed to analyze the XAS data. First, the raw absorption spectrum in the pre-edge region was fitted to a straight line, and the background above the edge was fitted with a cubic spline. The EXAFS function, χ, was obtained by subtracting the postedge background from the overall absorption and then normalized with respect to the edge jump step. The normalized $\chi(E)$ was transformed from energy space to **k** space, where **k** is the photoelectron wave vector. The $\chi(\mathbf{k})$ data were multiplied by $\mathbf{k}^3$ to compensate the damping of EXAFS oscillations in the high **k** region. Subsequently, and the $\mathbf{k}^3$-weighted $\chi(\mathbf{k})$ data in the **k** space ranging from 3.2 to 13.4 Å were Fourier transformed to **r** space to separate the EXAFS contributions from different coordination shells.

Cell Viability Assays

Compound exposure: Stock solutions of **2** were prepared in water. For the dose–response curves, cells were plated at 5000 cells well^{-} in 96-well plates. Media were removed 24 h after platting and replaced with a fresh one containing 0–500 μM of compound **2** or water (vehicle control).

Viability assays: After 48 h of cell incubation in the presence or absence of **2**, cell viability was evaluated with CellTiter 96 AQueous Non-Radioactive Cell Proliferation Assay (Promega, Madison, WI, USA) by MTS as previously described.[4]

Statistical analysis: All data were expressed as mean ± SEM from at least three independent experiments. Statistical significance was evaluated by using the Student's t-test; $p<0.05$ was considered statistically significant.

Acknowledgements

This work was partially supported by the Fundação para a Ciência e a Tecnologia (FCT), Portugal, and its PTDC/QUI-QUI/102150/2008, PTDC/EQU-EQU/122025–2010, PTDC/QUI-QUI/119561/2010, and PEst-OE/QUI/UI0100/2013 projects, and the National Science Council (NSC) of Taiwan (100-2221-E-011-105-MY3). T.F.S.S. is grateful to FCT for her Ph.D. (SFRH/BD/48087/2008) fellowship. The authors gratefully acknowledge Dr. Maria Cândida Vaz (IST) for the direction of the elemental analysis service, the Portuguese NMR Network (IST-UTL Center) for providing access to the NMR facility, and the Portuguese MS Network (IST Node) for the ESI measurements. M.L.K. thanks the FCT for the grant SFRH/BPD/88473/2012 and the FCT and IST for the research contract within the "FCT Investigator" scientific program. The facilities from the National Taiwan University of Science and Technology and National Synchrotron Radiation Research Center (NSRRC) are also acknowledged.

[1] a) S. Trofimenko, *Scorpionates, The Coordination Chemistry of Polypyrazolylborate Ligands*, Imperial College Press, London, **1999**; b) C. Pettinari, *Scorpionates II: Chelating Borate Ligands*, Imperial College Press, London, **2008**; c) D. L. Reger, T. C. Grattan, *Synthesis* **2003**, 0350–0356; d) R. V. Bernhardt, G. A. Lawrence, *Comprehensive Coordination Chemistry II*, *Vol. 6* (Eds.: J. A. McCleverty, T. J. Meyer), Elsevier, Oxford, **2004**, Ch. 6; e) B. Kräutler, *Encyclopedia of Inorganic Chemistry*, *Vol. II*, *2nd ed.* (Ed.: R. B. King), Wiley-VCH, Weinheim, **2005**.

[2] a) C. Pettinari, C. Santini, "Polypyrazolylborate and Scorpionate Ligands" in *Comprehensive Coordination Chemistry II: From Biology to Nanotechnology*, *Vol. 1* (Eds.: J. A. McCleverty, T. J. Meyer), Elsevier Pergamon (APS), Amsterdam, **2003**, pp. 159–210; b) C. Pettinari, R. Pettinari, *Coord. Chem. Rev.* **2005**, *249*, 525–543; c) H. R. Bigmore, C. S. Lawrence, P. Mountford, C. S. Tredget, *Dalton Trans.* **2005**, 635–651; d) A. Otero, J. Fernández-Baeza, A. Lara-Sánchez, L. F. Sánchez-Barba, *Coord. Chem. Rev.* **2013**, *257*, 1806–1868.

[3] a) F. Marchetti, C. Pettinari, R. Pettinari, A. Cerquetella, L. M. D. R. S. Martins, M. F. C. Guedes da Silva, T. F. S. Silva, A. J. L. Pombeiro, *Organometallics* **2011**, *30*, 6180–6188; b) C. Pettinari, F. Marchetti, G. Lupidi, L. Quassinti, M. Bramucci, D. Petrelli, L. A. Vitali, M. F. C. Guedes da Silva, L. M. D. R. S. Martins, P. Smoleński, A. J. L. Pombeiro, *Inorg. Chem.* **2011**, *50*, 11173–11183; c) T. F. S. Silva, M. F. C. Guedes da Silva, G. S. Mishra, L. M. D. R. S. Martins, A. J. L. Pombeiro, *J. Organomet. Chem.* **2011**, *696*, 1310–1318; d) R. Wanke, M. F. C. Guedes da Silva, S. Lancianesi, T. F. S. Silva, L. M. D. R. S. Martins, C. Pettinari, A. J. L. Pombeiro, *Inorg. Chem.* **2010**, *49*, 7941–7952; e) C. Dinoi, M. F. C. Guedes da Silva, E. C. B. A. Alegria, P. Smoleński, L. M. D. R. S. Martins, R. Poli, A. J. L. Pombeiro, *Eur. J. Inorg. Chem.* **2010**, 2415–2424; f) T. F. S. Silva, K. V. Luzyanin, M. V. Kirilova, M. F. C. Guedes da Silva, L. M. D. R. S. Martins, A. J. L. Pombeiro, *Adv. Synth. Catal.* **2010**, *352*, 171–187; g) T. F. S. Silva, G. S. Mishra, M. F. C. Guedes da Silva, R. Wanke, L. M. D. R. S. Martins, A. J. L. Pombeiro, *Dalton Trans.* **2009**, 9207–9215; h) G. S. Mishra, T. F. S. Silva, L. M. D. R. S. Martins, A. J. L. Pombeiro, *Pure Appl. Chem.* **2009**, *81*, 1217–1227; i) R. Wanke, P. Smoleński, M. F. C. Guedes da Silva, L. M. D. R. S. Martins, A. J. L. Pombeiro, *Inorg. Chem.* **2008**, *47*, 10158–10168; j) G. S. Mishra, E. C. B. A. Alegria, L. M. D. R. S. Martins, J. J. R. Fraústo da Silva, A. J. L. Pombeiro, *J. Mol. Catal. A* **2008**, *285*, 92–100; k) T. F. S. Silva, E. C. B. A. Alegria, L. M. D. R. S. Martins, A. J. L. Pombeiro, *Adv. Synth. Catal.* **2008**, *350*, 706–716; l) E. C. B. Alegria, M. V. Kirillova, L. M. D. R. S. Martins, A. J. L. Pombeiro, *Appl. Catal. A* **2007**, *317*, 43–52; m) T. F. S. Silva, L. M. D. R. S. Martins, M. F. C. Guedes da Silva, A. J. L. Pombeiro, *Acta Crystallogr. Sect. E* **2007**, *63*, m1979; n) E. C. B. A. Alegria, L. M. D. R. S. Martins, M. Haukka, A. J. L. Pombeiro, *Dalton Trans.* **2006**, 4954–4961; o) E. C. B. A. Alegria, L. M. D. R. S. Martins, M. F. C. Guedes da Silva, A. J. L. Pombeiro, *J. Organomet. Chem.* **2005**, *690*, 1947–1958; p) T. F. S. Silva, T. C. O. Mac Leod, L. M. D. R. S. Martins, M. F. C. Guedes da Silva, A. J. L. Pombeiro, *J. Mol. Catal. A* **2013**, *367*, 52–60; q) L. M. D. R. S. Martins, E. C. B. A. Alegria, P. Smoleński, M. L. Kuznetsov, A. J. L. Pombeiro, *Inorg. Chem.* **2013**, *52*, 4534–4546; r) L. M. D. R. S. Martins, A. Martins, E. C. B. A. Alegria, A. P. Carvalho, A. J. L. Pombeiro, *Appl. Catal. A* **2013**, *464–465*, 43–50; s) L. M. D. R. S. Martins, M. P. Almeida, S. A. C. Carabineiro, J. L. Figueiredo, A. J. L. Pombeiro, *ChemCatChem* **2013**, DOI: 10.1002/cctc.201300432; t) M. P. de Almeida, L. M. D. R. S. Martins, S. A. C. Carabineiro, T. Lauterbach, F. Rominger, A. S. K. Hashmi, A. J. L. Pombeiro, J. L. Figueiredo, *Catal. Sci. Technol.* **2013**, *3*, 3056–3069.

[4] T. F. S. Silva, L. M. D. R. S. Martins, M. F. C. Guedes da Silva, A. R. Fernandes, A. Silva, P. M. Borralho, S. Santos, C. M. P. Rodrigues, A. J. L. Pombeiro, *Dalton Trans.* **2012**, *41*, 12888–12897.

[5] a) E. I. Solomon, B. Hedman, K. O. Hodgson, A. Dey, R. K. Szilagyi, *Coord. Chem. Rev.* **2005**, *249*, 97–129; b) F. M. F. de Groot, *Inorg. Chim. Acta* **2008**, *361*, 850–856.

[6] H. Chao, L.-N. Hi, *Metallotherapeutic Drugs and Metal-Based Diagnostic Agents: The Use of Metals in Medicine* (Eds.: M. Gielen, E. R. T. Tiekink), Wiley, England, **2005**, Ch. 11.

[7] U. Jungwirth, C. Kowol, B. K. Keppler, C. G. Hartinger, W. Berger, P. Heffeter, *Antioxid. Redox Signaling* **2011**, *15*, 1085–1127.

[8] M. Frezza, S. Hindo, D. Chen, A. Davenport, S. Schmitt, D. Tomco, Q. P. Dou, *Curr. Pharm. Des.* **2010**, *16*, 1813–1825.

[9] D. Beyersmann, A. Hartwig, *Arch. Toxicol.* **2008**, *82*, 493–512.

[10] E. Kopera, T. Schwerdtle, A. Hartwig, W. Bal, *Chem. Res. Toxicol.* **2004**, *17*, 1452–1458.
[11] F. K. Keter, J. Darkwa, *Biometals* **2012**, *25*, 9–21.
[12] M. A. Cinellu, S. Stoccorro, G. Minghetti, A. L. Bandini, G. Bandi-telli, B. Bovio, *J. Organomet. Chem.* **1989**, *372*, 311–325.
[13] a) A. B. P. Lever, *Inorg. Chem.* **1990**, *29*, 1271–1285; b) A. B. P. Lever, *Comprehensive Coordination Chemistry II*, *Vol. 2* (Ed.: A. B. P. Lever), Elsevier, Oxford, **2004**, Ch. 2.19, pp. 251–268 and references cited therein; c) A. J. L. Pombeiro, *Encyclopaedia of Electrochemistry*, *Vol. 7A* (Eds.: F. Scholz, C. J. Pickett), Wiley-VCH, New York, **2006**, Ch. 6, pp. 77–108 and references cited therein; d) A. J. L. Pombeiro, *Eur. J. Inorg. Chem.* **2007**, 1473–1482; e) A. J. L. Pombeiro, *J. Organomet. Chem.* **2005**, *690*, 6021–6040; f) E. Reisner, V. B. Arion, A. Eichinger, N. Kandler, G. Geister, A. J. L. Pombeiro, B. K. Keppler, *Inorg. Chem.* **2005**, *44*, 6704–6716; g) A. I. F. Venâncio, M. L. Kuznetsov, M. F. C. Guedes da Silva, L. M. D. R. S. Martins, J. J. R. Fraústo da Silva, A. J. L. Pombeiro, *Inorg. Chem.* **2002**, *41*, 6456–6467.
[14] D. J. Harding, P. Harding, R. Daengngern, S. Yimklan, H. Adams, *Dalton Trans.* **2009**, 1314–1320.
[15] a) C. Di Nicola, Y. Y. Karabach, A. M. Kirillov, M. Monari, L. Pandolfo, C. Pettinari, A. J. L. Pombeiro, *Inorg. Chem.* **2007**, *46*, 221–230; b) D. S. Nesterov, V. N. Kokozay, V. V. Dyakonenko, O. V. Shishkin, J. Jezierska, A. Ozarowski, A. M. Kirillov, M. N. Kopylovich, A. J. L. Pombeiro, *Chem. Commun.* **2006**, 4605–4607; c) A. M. Kirillov, M. N. Kopylovich, M. V. Kirillova, E. Y. Karabach, M. Haukka, M. F. C. Guedes da Silva, A. J. L. Pombeiro, *Adv. Synth. Catal.* **2006**, *348*, 159–174; d) A. M. Kirillov, M. N. Kopylovich, M. V. Kirillova, M. Haukka, M. F. C. Guedes da Silva, A. J. L. Pombeiro, *Angew. Chem.* **2005**, *117*, 4419–4423; *Angew. Chem. Int. Ed.* **2005**, *44*, 4345–4349; e) A. M. Kirillov, M. Haukka, M. F. C. Guedes da Silva, A. J. L. Pombeiro, *Eur. J. Inorg. Chem.* **2005**, 2071–2080; f) M. N. Kopylovich, A. M. Kirillov, A. K. Baev, A. J. L. Pombeiro, *J. Mol. Catal. A* **2003**, *206*, 163–168; g) P. M. Reis, J. A. L. Silva, J. J. R. Fraústo da Silva, A. J. L. Pombeiro, *Chem. Commun.* **2000**, 1845–1846; h) M. V. Kirillova, M. L. Kuznetsov, P. M. Reis, J. A. L. Silva, J. J. R. Fraústo da Silva, A. J. L. Pombeiro, *J. Am. Chem. Soc.* **2007**, *129*, 10531–10545; i) M. V. Kirillova, M. L. Kuznetsov, J. A. L. Silva, M. F. C. Guedes da Silva, J. J. R. Fraústo da Silva, A. J. L. Pombeiro, *Chem. Eur. J.* **2008**, *14*, 9312–9322; j) R. R. Fernandes, M. V. Kirillova, J. A. L. Silva, J. J. R. Fraústo da Silva, A. J. L. Pombeiro, *Appl. Catal. A* **2009**, *353*, 107–112.
[16] a) G. B. Shul'pin, *C. R. Chim.* **2003**, *6*, 163–178; b) G. B. Shul'pin, *J. Mol. Catal. A* **2002**, *189*, 39–66; c) G. B. Shul'pin, Y. N. Kozlov, G. V. Nizova, G. Süss-Fink, S. Stanislas, A. Kitaygorodskiy, V. S. Kulikova, *J. Chem. Soc. Perkin Trans. 2* **2001**, 1351–1357; d) G. B. Shul'pin, G. Süss-Fink, J. R. L. Smith, *Tetrahedron* **1999**, *55*, 5345–5358.
[17] a) M. V. Kirillova, M. L. Kuznetsov, V. B. Romakh, L. S. Shul'pina, J. J. R. Fraústo da Silva, A. J. L. Pombeiro, G. B. Shul'pin, *J. Catal.* **2009**, *267*, 140–157; b) M. V. Kirillova, A. M. Kirillov, M. F. C. Guedes da Silva, A. J. L. Pombeiro, *Eur. J. Inorg. Chem.* **2008**, 3423–3427; c) M. V. Kirillova, A. M. Kirillov, P. M. Reis, J. A. L. Silva, J. J. R. Fraústo da Silva, A. J. L. Pombeiro, *J. Catal.* **2007**, *248*, 130–136.
[18] a) M. L. Kuznetsov, A. J. L. Pombeiro, *Inorg. Chem.* **2009**, *48*, 307–318; b) M. V. Kirillova, M. L. Kuznetsov, Y. N. Kozlov, L. S. Shul'pina, A. Kitaygorodskiy, A. J. L. Pombeiro, G. B. Shul'pin, *ACS Catal.* **2011**, *1*, 1511–1520; c) M. V. Kirillova, Y. N. Kozlov, L. S. Shul'pina, O. Y. Lyakin, A. M. Kirillov, E. P. Talsi, A. J. L. Pombeiro, G. B. Shul'pin, *J. Catal.* **2009**, *268*, 26–38.
[19] *X-Ray Absorption: Principles, Applications, Techniques of EXAFS, SEXAFS and XANES* (Eds.: D. C. Konningsberger, R. Prins), Wiley, New York, **1988**, p. 362.
[20] H. C. Choi, S. Y. Lee, S. B. Kim, M. G. Kim, M. K. Lee, H. J. Shin, J. S. Lee, *J. Phys. Chem. B* **2002**, *106*, 9252–9260.
[21] C.-W. Yu, K. K. W. Li, S.-K. Pang, S. C. F. Au-Yeung, Y.-P. Ho, *Bioorg. Med. Chem. Lett.* **2006**, *16*, 1686–1691.
[22] L. T. Vassilev, B. T. Vu, B. Graves, D. Carvajal, F. Podlaski, Z. Filipovic, N. Kong, U. Kammlott, C. Lukacs, C. Klein, N. A. Fotouhi, E. A. Liu, *Science* **2004**, *303*, 844–848.
[23] E. Reisner, V. B. Arion, B. K. Keppler, A. J. L. Pombeiro, *Inorg. Chim. Acta* **2008**, *361*, 1569–1583.
[24] N. Graf, S. J. Lippard, *Adv. Drug Delivery Rev.* **2012**, *64*, 993–1004.
[25] a) A. J. L. Pombeiro, M. F. C. Guedes da Silva, M. A. N. D. A. Lemos, *Coord. Chem. Rev.* **2001**, *219*, 53–80; b) M. E. N. P. R. A. Silva, A. J. L. Pombeiro, J. J. R. Fraústo da Silva, R. Herrmann, N. Deus, T. J. Castilho, M. F. C. Guedes da Silva, *J. Organomet. Chem.* **1991**, *421*, 75–90.
[26] a) Bruker, *APEX2& SAINT*; AXS, Inc., Madison, WI, **2004**; b) G. M. Sheldrick, *Acta Crystallogr. Sect. A* **2008**, *64*, 112–122; c) L. J. Farrugia, *J. Appl. Crystallogr.* **1999**, *32*, 837–838.
[27] a) A. D. Becke, *J. Chem. Phys.* **1993**, *98*, 5648–5652; b) C. Lee, W. Yang, R. G. Parr, *Phys. Rev. B* **1988**, *37*, 785–789.
[28] Gaussian 09, revision A.01, M. J. Frisch, G. W. Trucks, H. B. Schlegel, G. E. Scuseria, M. A. Robb, J. R. Cheeseman, G. Scalmani, V. Barone, B. Mennucci, G. A. Petersson, H. Nakatsuji, M. Caricato, X. Li, H. P. Hratchian, A. F. Izmaylov, J. Bloino, G. Zheng, J. L. Sonnenberg, M. Hada, M. Ehara, K. Toyota, R. Fukuda, J. Hasegawa, M. Ishida, T. Nakajima, Y. Honda, O. Kitao, H. Nakai, T. Vreven, J. A. Montgomery, Jr., J. E. Peralta, F. Ogliaro, M. Bearpark, J. J. Heyd, E. Brothers, K. N. Kudin, V. N. Staroverov, R. Kobayashi, J. Normand, K. Raghavachari, A. Rendell, J. C. Burant, S. S. Iyengar, J. Tomasi, M. Cossi, N. Rega, J. M. Millam, M. Klene, J. E. Knox, J. B. Cross, V. Bakken, C. Adamo, J. Jaramillo, R. Gomperts, R. E. Stratmann, O. Yazyev, A. J. Austin, R. Cammi, C. Pomelli, J. W. Ochterski, R. L. Martin, K. Morokuma, V. G. Zakrzewski, G. A. Voth, P. Salvador, J. J. Dannenberg, S. Dapprich, A. D. Daniels, O. Farkas, J. B. Foresman, J. V. Ortiz, J. Cioslowski, D. J. Fox, Gaussian, Inc., Wallingford, CT, **2009**.
[29] a) L. Noodleman, D. A. Case, *Adv. Inorg. Chem.* **1992**, *38*, 423–470; b) E. Ruiz, J. Cano, S. Alvarez, P. Alemany, *J. Comput. Chem.* **1999**, *20*, 1391–1400; c) E. Ruiz, A. Rodriguez-Fortea, J. Cano, S. Alvarez, P. Alemany, *J. Comput. Chem.* **2003**, *24*, 982–989; d) A. P. Ginsberg, *J. Am. Chem. Soc.* **1980**, *102*, 111–117; e) L. Noodleman, *J. Chem. Phys.* **1981**, *74*, 5737–5743; f) L. Noodleman, E. R. Davidson, *Chem. Phys.* **1986**, *109*, 131–143; g) T. Soda, Y. Kitagawa, T. Onishi, Y. Takano, Y. Shigeta, H. Nagao, Y. Yoshioka, K. Yamaguchi, *Chem. Phys. Lett.* **2000**, *319*, 223–230.
[30] M. Dolg, U. Wedig, H. Stoll, H. Preuss, *J. Chem. Phys.* **1987**, *86*, 866–872.
[31] A. Silva, D. Luís, S. Santos, J. Silva, A. S. Mendo, L. Coito, T. F. S. Silva, M. F. C. Guedes da Silva, L. M. D. R. S. Martins, A. J. L. Pombeiro, P. Borralho, M. C. M. Rodrigues, M. G. Cabral, P. A. Videira, C. Monteiro, A. R. Fernandes, *Drug Metab. Drug Interact.* **2013**, *28*, 167–176.

Received: October 4, 2013
Revised: December 1, 2013
Published online: January 30, 2014